Decreased Northern Hemisphere Precipitation from Consecutive CO_2 Doublings Is Associated with Significant AMOC Weakening

X. Zhang[1], D. W. Waugh[2], I. Mitevski[3], C. Orbe[4,5], and L. M. Polvani[5,6]

[1]Department of Physics, University of Nevada, Reno, NV, USA.
[2]Department of Earth and Planetary Sciences, Johns Hopkins University, Baltimore, MD, USA.
[3]Department of Geosciences, Princeton University, Princeton, NJ, USA.
[4]NASA Goddard Institute for Space Studies, New York, NY, USA.
[5]Department of Applied Physics and Applied Mathematics, Columbia University, New York, NY, USA.
[6]Lamont-Doherty Earth Observatory, Columbia University, Palisades, NY, USA.

E-mail: xiyuez@unr.edu

Abstract

Previous studies found many climate properties such as northern hemisphere (NH) surface temperature and precipitation respond non-monotonically when CO_2 is increased from 1x to 8xCO_2 relative to pre-industrial levels. Here, we explore the robustness of the non-monotonicity in the NH precipitation response in 11 coupled climate models. Eight models show a decrease in NH precipitation under repeated CO_2 doubling, indicating that the non-monotonic response is a common but not universal result. Although common, the critical CO_2 level where the NH precipitation decrease first occurs differs widely across models, ranging from 2xCO_2 to 8xCO_2. These models also show a prominent weakening in the Atlantic meridional overturning circulation (AMOC) at the same critical CO_2 level, with the AMOC weakening leading the precipitation decrease. The sensitivities of NH precipitation and the AMOC to CO_2 doublings are positively correlated, especially when the AMOC weakens beyond 10 Sv. This suggests that the differences in models' AMOC response can explain their contrasting NH precipitation responses, where models with a large AMOC weakening have decreased NH precipitation. Regionally, this decrease in NH precipitation is the most prominent over the North Atlantic, Europe and the tropical Pacific. Our results suggest that special care must be taken with the use of pattern scaling to inform regional climate decision-making.

Keywords: precipitation, abrupt CO_2 increase, AMOC, climate change

1. Introduction

In a recent study, Mitevski et al. (2021, hereafter M21) found non-monotonic responses of a range of climate properties to CO_2 forcing in two fully coupled climate models. Specifically, they reported decreased northern hemisphere (NH) surface temperature, expanded Arctic sea ice extent, reduced NH precipitation, contracted subtropical dry zones, and a stronger NH Hadley cell with increasing CO_2 beyond some threshold value, in abrupt forcing simulations spanning 1–8xCO_2. While this surprising behavior was found in both models, the threshold CO_2 concentration beyond which it occurred was different between the two models: it appeared between 2xCO_2 and 3xCO_2 for one model, but between 3xCO_2 and 4xCO_2 for the other model.

The mechanisms behind the non-monotonic response to CO_2 increase have also been explored. M21 found that the non-monotonicity is not present in the slab-ocean versions of the same models, clearly implicating a key role for ocean dynamics. Subsequent studies (Mitevski et al., 2022, 2023; Orbe et al., 2023) showed that such ocean dynamics are related to cooling over the North Atlantic (the North Atlantic warming hole, NAWH) and a concurrent weakening of the Atlantic meridional overturning circulation (AMOC). Multiple North Atlantic "hosing" experiments have demonstrated that a weakened AMOC leads to the NAWH, decreased precipitation over the NH, and a southward shift of the ITCZ in coupled climate models (R. Zhang & Delworth, 2005; Stouffer et al., 2006; Jackson et al., 2015; Liu et al., 2020). The NAWH not only reduces local SSTs and the NH atmospheric moisture content (Jackson et al., 2015), but also strengthens the meridional SST gradient and changes the cross-equatorial atmospheric heat transport (Moreno-Chamarro et al., 2019), which explain the NH precipitation decrease.

This non-monotonic response has important implications when extrapolating results from 4xCO_2 simulations to other levels of CO_2 forcing (Chadwick & Good, 2013). A particular application is the use of "pattern scaling" that provides quantitative decision-relevant climate information on a regional scale over a range of scenarios (e.g., Lopez et al., 2014). Furthermore, given the difference in CO_2 levels at which the non-monotonicity appears, it represents a plausible source of uncertainty in the model spread in response to 4xCO_2 forcing (e.g., Grise & Polvani, 2016). However, there are several outstanding questions to be answered before examining how the non-monotonicity contributes to the inter-model spread of the atmospheric circulation response to 4xCO_2 forcing. First of all, it is not known whether the non-monotonicity occurs in all models, and how widely the critical CO_2 level varies across models. Furthermore, the robustness of the connection to the AMOC has only been recently explored in one climate model (Orbe et al., 2023).

Here, we answer these questions by examining the response of NH precipitation, NAWH temperature, and the AMOC using models with abrupt 2xCO_2 and 4xCO_2 forcing simulations as part of the Coupled Model Intercomparison Project Phase 6 (CMIP6, Eyring et al., 2016), as well as models with abrupt 2xCO_2, 4xCO_2, and 8xCO_2 forcing simulations available from LongrunMIP (Rugenstein et al., 2019). We focus on NH precipitation as this field is available in all simulations (LongrunMIP has limited variables archived). Furthermore, a non-monotonic NH precipitation response is a good indicator of non-monotonic behavior in other circulation metrics as demonstrated by M21. In addition to NH averaged precipitation, we separately examine the precipitation response in the extratropical, subtropical, and deep tropical regions, to identify where the non-monotonicity is the most evident. We also analyze the spatial pattern of the precipitation response composited at critical and non-critical CO_2 levels.

2. Data and Methods

We analyze the output from 11 coupled climate models for which there are 150 years of simulations with an abrupt doubling and quadrupling of CO_2 from pre-industrial levels (Table 1).

Models	**Pre-Industrial ($1xCO_2$)**	**$2xCO_2$**	**$4xCO_2$**	**$8xCO_2$**	**Simulation References**
GISS-E2.1	x, s	x, s	x [c], s	x [n]	Mitevski et al. (2021)
CESM1	x, s	x, s	x [c], s	x [n]	Mitevski et al. (2021)
CESM2	x	x [c]	x [n]		CMIP6/CFMIP-3
MRI-ESM2-0	x	x [c]	x [n]		CMIP6/CFMIP-3
CanESM5	x	x	x		CMIP6/CFMIP-3
HadCM3L	x	x	x [n]	x [c]	LongrunMIP
CESM104	x	x	x	x	LongrunMIP
MPIESM12	x	x	x	x	LongrunMIP
GISS-E2.2-OMA	x	x [c]	x [n]		CMIP6/CFMIP-3
GISS-E2.2-NINT	x	x [n]	x [c]		CMIP6/CFMIP-3
GISS-E2.2-LINOZ	x	x [c]	x [n]	x	Orbe et al. (2024)

Table 1 . Model simulations used in this study. An x indicates the availability of output from coupled models. An "s" indicates the availability of output from the slab-ocean configuration of the models. Critical CO_2 levels are indicated with [c]. Non-critical CO_2 level simulations used for composites on Figure 3 and 5 are indicated with [n].

For six of these models, abrupt $8xCO_2$ simulations are also available. This suite includes the two models (GISS-E2.1 and CESM1) analyzed in M21, five models (CESM2, MRI-ESM2-0, CanESM5, and GISS-E2.2-OMA and GISS-E2.2-NINT) from the Cloud Feedback Model Intermodal Comparison phase 3 (CFMIP-3, Webb et al., 2017) with ocean overturning streamfunction output available, and three models (HadCM3L, CESM104, and MPIESM12) from LongrunMIP (Rugenstein et al., 2019). We also include output from GISS-E2.2-LINOZ simulations (Orbe et al., 2024), where the abrupt $2xCO_2$ simulation is 140 years long. The CMIP6 archive includes two versions of GISS-E2.2 that differ in their treatment of atmospheric chemistry (the NINT version "physics version 1" has no interactive chemistry and the OMA version "physics version 3" has full tropospheric and stratospheric chemistry). GISS-E2.2-LINOZ has linearized stratospheric ozone chemistry but non-interactive tropospheric chemistry or aerosols. We also include the slab ocean model (SOM) versions of the 60-year pre-industrial, abrupt $2xCO_2$ and $4xCO_2$ simulations from GISS-E2.1 and CESM1 (M21).

We calculate the averages of the last 50 years of the abrupt CO_2 simulations and 50 years of the pre-industrial simulations to represent the quasi-equilibrium states of each simulation in all models. We assess the significance of the equilibrium state for each simulation by showing the range of the 50-year mean values at 95% confidence interval using a Student's *t*-distribution. The variables of interest include precipitation (P), surface temperature (T_s), and the AMOC. We focus on the NH-averaged precipitation (P_{NH}), T_s averaged over the NAWH region (45ºN–65ºN, 40ºW–20ºW) (T_{NAWH}), and the strength of the AMOC (ψ_{AMOC}, defined in M21 as the maximum Atlantic ocean overturning streamfunction between 30ºN–55ºN and 800–2000 m). The last 30 years are averaged to represent the response for slab ocean simulations.

In a similar manner to Good et al. (2016), we calculate the sensitivity of a quantity X to a CO_2 doubling by computing

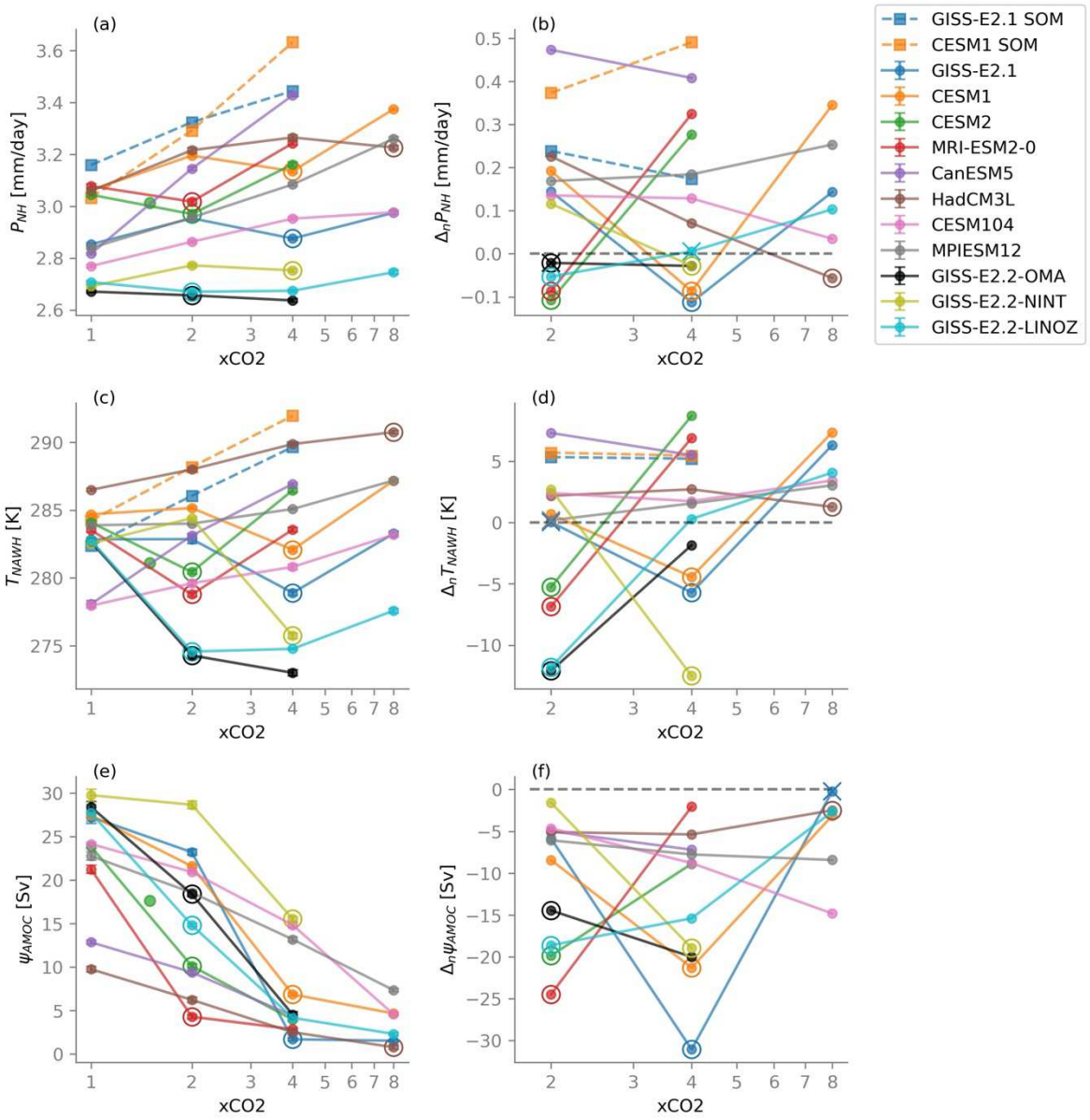

Figure 1 Annual mean NH climate properties as functions of CO_2 forcing (x-axis on log scale). (a) NH precipitation (P_{NH}), (b) NH precipitation sensitivity $\Delta_n P_{NH}$ to CO_2 doubling, (c) North Atlantic warming hole surface temperature (T_{NAWH}), (d) NAWH temperature sensitivity $\Delta_n T_{NAWH}$ to CO_2 doubling, (e) AMOC strength (ψ_{AMOC}), and (f) AMOC sensitivity $\Delta_n \psi_{AMOC}$ to CO_2 doubling. An additional CESM2 1.5xCO_2 simulation is shown in green dots. Slab ocean model (SOM) simulations are shown in dashed squares. Circles indicate simulations at the critical CO_2 levels where a decrease of P_{NH} to CO_2 doubling first occur. Error bars on the left panels indicate the range of the 50-year mean values at 95% confidence interval using a Student's *t*-distribution. Crosses on the right panels show sensitivities that are not statistically significant at 95% confidence interval.

$$\Delta_n X = X(n \times CO_2) - X\left(\frac{n}{2} \times CO_2\right),$$

where $X = (P_{NH}, T_{NAWH}, \psi_{AMOC})$ and $X(n \times CO_2)$ is X for the abrupt $n \times CO_2$ simulation. For example, $\Delta_4 P_{NH} = P_{NH}(4 \times CO_2) - P_{NH}(2 \times CO_2)$ is the change in NH-averaged precipitation between doubling and quadrupling CO_2. We calculate $\Delta_n X$ for $n = 2$, 4, and 8 (when available). The significance of the sensitivity is assessed by comparing the two 50-year X samples using a two-sided Student's t-test at 95% confidence interval.

Assuming the CO_2 radiative forcing is a linear function of ln ($n \times CO_2/1 \times CO_2$) (e.g., Myhre et al., 1998), if the response of X scales with radiative forcing then it will be also be linear with ln ($n \times CO_2/1 \times CO_2$). If so, $\Delta_n X$ will then be identical for all n, i.e., $\Delta_2 X = \Delta_4 X = \Delta_8 X$, and nonlinearity can be diagnosed by the difference in $\Delta_n X$ for different values of n. Here, our primary interest is the occurrence of non-monotonic responses to radiative forcing, which implies $\Delta_n X$ changes sign for increasing n. Because one expects an increase in global-mean P with increasing CO_2 (Pendergrass, 2020), we focus here on the surprising occurrence of a decrease in P_{NH} under CO_2 doubling. In models where this occurs, we define the critical CO_2 level as the lowest value of n for which $\Delta_n P_{NH}$ is negative, i.e. if $\Delta_2 P_{NH} < 0$ for a model, then the critical CO_2 level for that model is 2xCO_2. We average simulations at the critical CO_2 levels to produce multi-model mean time series of ψ_{AMOC}, P_{NH}, T_{NAWH} and maps of $\Delta_n T_{NAWH}$ and $\Delta_n P_{NH}$. For comparison, we also average simulations for adjacent non-critical CO_2 levels for each model (see Table 1). We use the $2n \times CO_2$ simulation for the non-critical CO_2 levels, but if it's not available we the $\frac{n}{2} \times CO_2$ simulation.

3. Results

3.1 NH precipitation, NAWH temperature, and AMOC responses

Among the models analyzed here, we have found a wide range of behavior in how P_{NH} responds to increased CO_2 (Figure 1a), notably in the sign and magnitude of the change in P_{NH} for a doubling of CO_2 (Figure 1b). Across all models and $n \times CO_2$, $\Delta_n P_{NH}$ varies from -0.12 to 0.47 mm/day, and 8 out of 11 models show $\Delta_n P_{NH} < 0$, for at least one n. Four models (CESM2, MRI-ESM2-0, GISS-E2.2-LINOZ, GISS-E2.2-OMA) show a decrease in P_{NH} first at $n = 2$ (although $\Delta_2 P_{NH}$ from GISS-E2.2-OMA is not statistically significant), three models (GISS-E2.1, CESM1, and GISS-E2.2-NINT) at $n = 4$, and one model(HadCM3L) at $n = 8$ (Figure 1b). While three models (CanESM5, CESM104, and MPIESM12) show a monotonic increase of P_{NH} from 2xCO_2 to 8xCO_2, the response to CO_2 doubling is still nonlinear, i.e., $\Delta_n P_{NH}$ varies with n (Figure 1b). This analysis, therefore, shows that while the M21 finding of a non-monotonic P_{NH} response is common, it is not universal. The non-monotonicity is also absent in slab ocean counterparts of GISS-E2.1 and CESM1 (Figure 1a). Moreover, it shows that there is a large spread among models in the critical CO_2 level for a decrease in P_{NH}. M21 showed that a decrease in P_{NH} occurred between 2xCO_2 and 3xCO_2 for GISS-E2.1, and between 3xCO_2 and 4xCO_2 for CESM1 (in our analysis, which considers only 2x and 4xCO_2, the critical CO_2 value is $n = 4$ for both models). However, Figures 1a and 1b show that in other models this critical value can also be 2xCO_2 or 8xCO_2. Furthermore, an additional 1.5xCO_2 simulation with CESM2 shows a decrease in P_{NH} from PI (Figure 1a), so a decrease in P_{NH} can occur below 2xCO_2.

M21 related the non-monotonic P_{NH} response to the non-monotonic response in NH-averaged T_s, and showed that it is only evident when the NAWH region is included. Consistent with this, we find a good correspondence between the T_{NAWH} and P_{NH} response in our suite of models (Figures 1c and 1d). One can see a generally good agreement in the relative magnitude of $\Delta_n P_{NH}$ and $\Delta_n T_{NAWH}$, with models with large $\Delta_n P_{NH}$ also having large $\Delta_n T_{NAWH}$ (including the slab ocean models). More importantly, models that show a decrease in P_{NH} for CO_2 doubling also show a decrease in T_{NAWH} at the same critical n (Figures 1b and 1d). HadCM3L is the exception, but note that $\Delta_8 T_{NAWH}$ is close to zero for that model, i.e., there is little increase in T_{NAWH} from 4x to 8xCO_2, which is where P_{NH} decreases in that model.

Several recent studies have linked nonlinearity in the atmospheric and T_{NAWH} responses to differences in the AMOC response (e.g., Bellomo et al., 2021; Mitevski et al., 2021, 2022, 2023; Orbe et al., 2023; Zhang et al., 2023). We also find

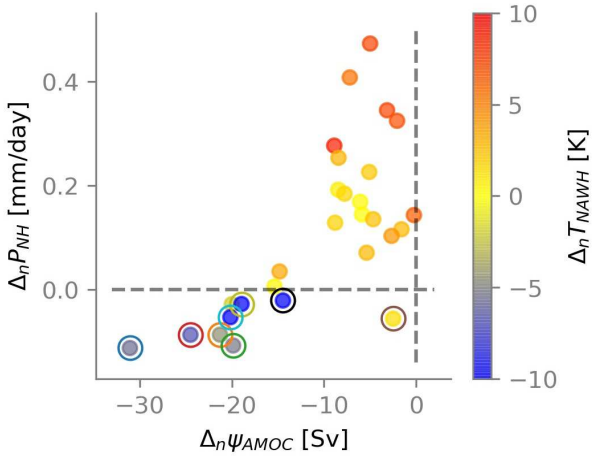

Figure 2 Scatter plots showing the relationship between AMOC sensitivity $\Delta_n \psi_{AMOC}$ and NH precipitation sensitivity $\Delta_n P_{NH}$ to CO_2 doubling. NAWH temperature sensitivity $\Delta_n T_{NAWH}$ is shown in colors. Circles indicate simulations at the critical CO_2 levels where a decrease of P_{NH} to CO_2 doubling first occurs (same as in Figure 1).

strong connections between the response in T_{NAWH} and P_{NH} and the response in ψ_{AMOC}. While all models show a ψ_{AMOC} decrease with increasing CO_2, the rate of the ψ_{AMOC} weakening varies greatly across models and with n (Figure 1e). This variation is closely linked with variations in the P_{NH} and T_{NAWH} responses. Models with a small decrease in ψ_{AMOC} under CO_2 doubling show an increase in T_{NAWH} and P_{NH}. Models with a large decrease in ψ_{AMOC} show T_{NAWH} and P_{NH} decreases, indicating that a collapsed AMOC is associated with a decrease in T_{NAWH} and P_{NH} (Figures 1b, 1d, and 1f). The $\Delta_n \psi_{AMOC}$ threshold for the different response is around -10 Sv, with $\Delta_n P_{NH} \leq 0$ and $\Delta_n T_{NAWH} \leq 0$ for $\Delta_n \psi_{AMOC} <$ -10 Sv, but $\Delta_n P_{NH} > 0$ and $\Delta_n T_{NAWH} > 0$ for $\Delta_n \psi_{AMOC} >$ -10 Sv. Again, HadCM3L is the exception, given that its pre-industrial ψ_{AMOC} is underestimated and around 10 Sv.

The interrelationships between $\Delta_n \psi_{AMOC}$, $\Delta_n T_{NAWH}$, and $\Delta_n P_{NH}$ are summarized in Figure 2. A positive correlation between $\Delta_n \psi_{AMOC}$ and $\Delta_n P_{NH}$ is evident (with explained variance $r^2 = 0.48, p < 0.001$), especially for $\Delta_n \psi_{AMOC} < -10$ Sv ($r^2 = 0.65, p < 0.01$). This suggests that a more negative $\Delta_n \psi_{AMOC}$ is associated with more negative $\Delta_n P_{NH}$ and $\Delta_n T_{NAWH}$. For $\Delta_n \psi_{AMOC} > -10$ Sv, $\Delta_n P_{NH}$ shows little dependence on $\Delta_n \psi_{AMOC}$. However, larger $\Delta_n P_{NH}$ is associated with larger $\Delta_n T_{NAWH}$. Therefore, when the decrease in ψ_{AMOC} is small, P_{NH} is largely influenced by other non-AMOC factors that can increase T_{NAWH}.

A closer look at the time series of ψ_{AMOC}, P_{NH}, and T_{NAWH} at the critical CO_2 levels offers insights into the evolution of these variables throughout the simulations (Figure 3). Particularly, we find a lead-lag relationship between their responses to abrupt CO_2 increase. The AMOC strength decreases immediately after the abrupt CO_2 increase, while both P_{NH} and T_{NAWH} increase in the first 10 years. Then T_{NAWH} decreases drastically, reaching its pre-industrial value around Year 20, and continues to decrease until it stabilizes around Year 100. This cooling clearly lags the weakening of the AMOC. While P_{NH} displays large interannual variability, its decreasing trend is apparent after Year 20, which further lags the cooling of T_{NAWH}. The persistent decrease of P_{NH} after the first 20 years of the simulations results in a negative precipitation sensitivity $\Delta_n P_{NH}$. While there are discernible inter-model differences in their ψ_{AMOC}, P_{NH}, and T_{NAWH} responses, there is a consistent picture of T_{NAWH} and P_{NH} decreases lagging behind the weakening of ψ_{AMOC} (Figure S1). This suggests a critical role the AMOC weakening plays in driving the decrease in NAWH and NH precipitation.

3.2 Regional precipitation response

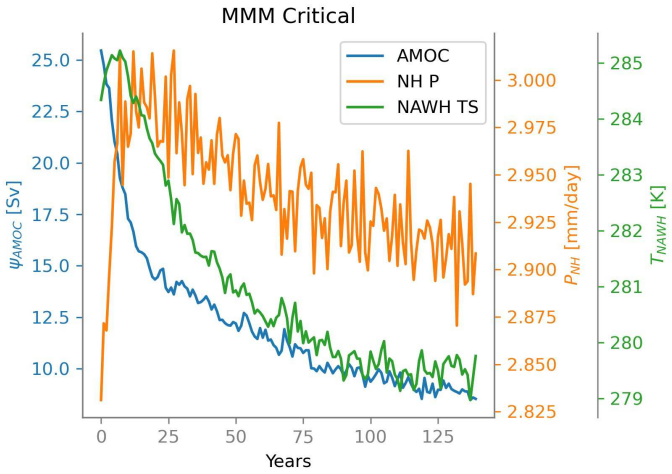

Figure 3 Multi-model mean time series of AMOC strength (ψ_{AMOC}), NAWH surface temperature (T_{NAWH}), and NH precipitation (P_{NH}) averaged over simulations at the critical CO_2 levels. See Table 1 for models at critical CO_2 levels.

The above shows that in most models there exists a critical CO_2 level beyond which P_{NH} decreases upon CO_2 doubling, and that such decrease is related to a decrease in T_{NAWH}. Now we ask: Is this decrease occurring across the entire NH, or is it limited to the cooling region around the NAWH? To explore this, we partition the P_{NH} response into the extratropical (30ºN–90ºN, P_{30-90N}), subtropical (5-30ºN, P_{5-30N}), and deep-tropical (0º-5ºN, P_{0-5N}) regions (Figure 4).

The response of P_{30-90N} to increasing CO_2 is similar to that of P_{NH} (Figure 4a). Models that have a decrease in P_{NH} also show a decrease in P_{30-90N} at the same nxCO_2, except for CESM2 and MRI-ESM2-0 where there is a slight increase, rather than decrease, in P_{30-90N} between 1xCO_2 and 2xCO_2. However, this increase is much less than the increase in P_{30-90N} between 2xCO_2 and 4xCO_2 for these two models, and their P_{30-90N} response is nonlinear. The response of P_{30-90N} largely scales with $T_{s,30-90N}$ response (Figure 4b). The majority of the models have a regression slope between the global-mean hydrological sensitivity of 2.5%/K (black dashed line, Pendergrass, 2020) and the Clausius-Clapeyron scaling of 7%/K (gray dashed line). Two models have deviations from this positive regression: GISS-E2.2-OMA shows invariant P_{30-90N} with $T_{s,30-90N}$ and HadCM3L at 8xCO_2 shows a slight negative slope.

While the P_{30-90N} response is similar to that of P_{NH}, it is notable that the decrease in P_{30-90N} at the critical CO_2 level is smaller in magnitude, indicating that precipitation must also decrease at lower latitudes. These decreases occur within the subtropics, where nearly all models show a general decrease in P_{5-30N} with increasing CO_2 (Figure 4c). This decrease is also manifested in negative regression slopes with $T_{s,5-30N}$ response across most models (Figure 4d). The decrease in P_{5-30N} is most prominent at the critical CO_2 levels (circles in Figure 4c), which suggests that subtropical drying under increased CO_2 is further exaggerated when the AMOC is significantly weakened. It is notable that the P_{5-30N} decrease at this forcing is much larger in magnitude than that for P_{30-90N}. In other words, most the decrease in P_{NH} is coming from the subtropics and not the extratropics.

As we move to the deep tropics, P_{0-5N} increases monotonically with CO_2 in all models (Figure 4e). The response of P_{0-5N} scales positively with $T_{s,0-5N}$ response at slopes much steeper than the Clausius-Clapeyron scaling (Figure 4f). Simulations at

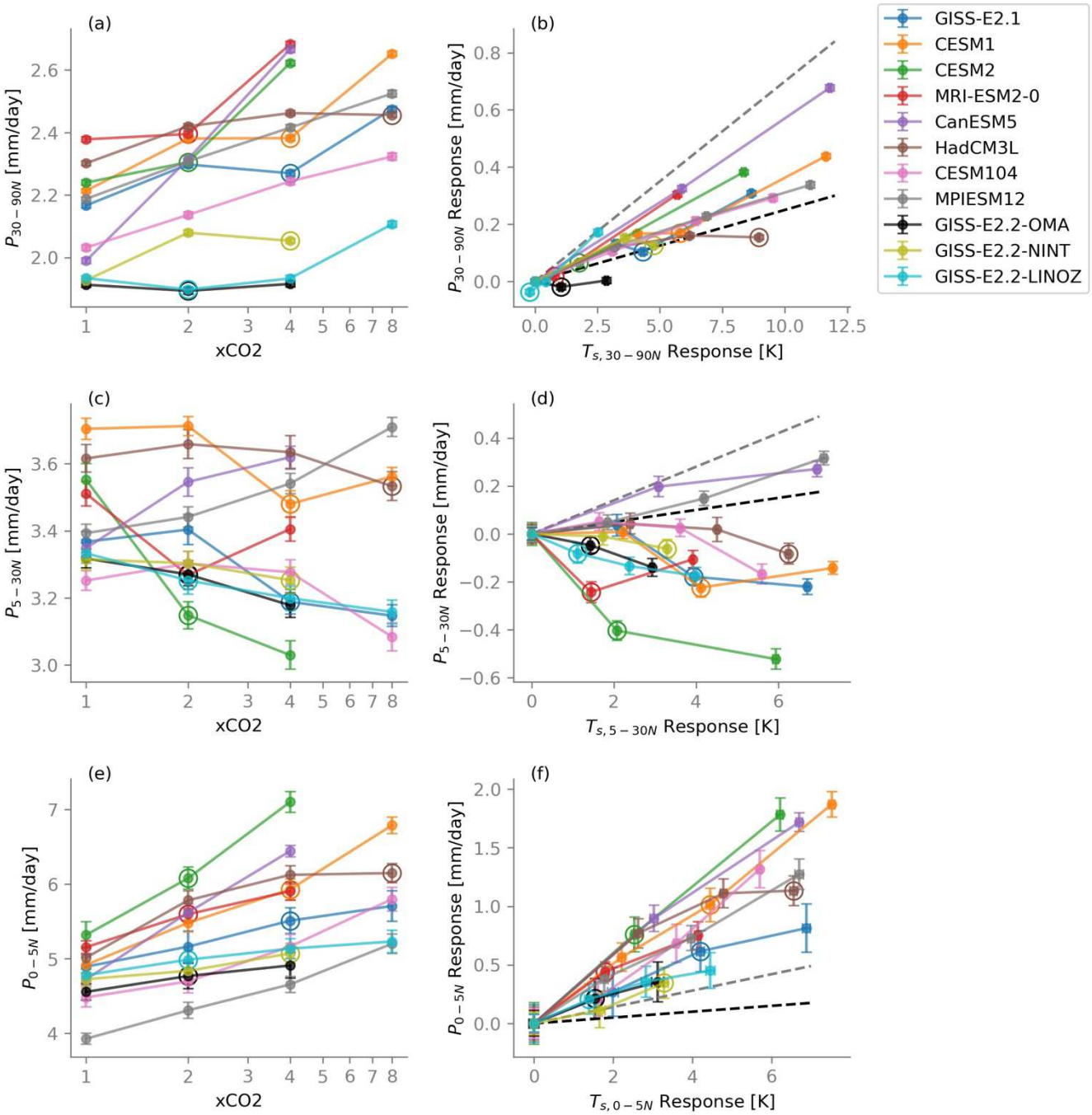

Figure 4 Annual-mean precipitation averaged over (a, b) extratropics 30º–90ºN, (c, d) subtropics (5º–30ºN), and (e, f) deep tropics (0º–5ºN). Left column shows precipitation as a function of CO_2 forcing (on *log* scale). Right column shows the precipitation response as a function of surface temperature response. Dashed lines on the right the global-mean hydrological sensitivity (2.5%/K, black) and the Clausius-Clapeyron scaling (7%/K, gray). Circles indicate simulations at the critical CO_2 levels where a decrease of P_{NH} for a doubling of CO_2 concentration first occurs. Error bars indicate the range of the 50-year mean values at 95% confidence interval using a Student's *t*-distribution.

the critical CO_2 level are not distinguishable from other simulations, except for HadCM3L at 8xCO_2. This suggests that P_{0-5N} is dominated by the response to CO_2 increase and less influenced by changes in ψ_{AMOC}.

The latitudinal difference in P response motivates us to look into the spatial patterns in more detail. We investigate composite maps of $\Delta_n T_s$ and $\Delta_n P$ averaged over 8 models that show a decrease in P_{NH} at their critical CO_2 levels (Figures 5a and 5b), and compare them to their adjacent non- critical CO_2 average (Figures 5c and 5d, see Table for adjacent non-critical CO_2 values for each model). Their differences quantify the spatial pattern of the nonlinear T_s and P responses (Figures 5e and 5f).

Models at critical CO_2 levels show strong cooling in the NAWH (Figure 5a) and have smaller Arctic amplification than models at non-critical CO_2 levels (Figure 5c). The difference between models at critical and non-critical levels is characterized by polar-amplified cooling that is the strongest over the NAWH and the Arctic Ocean (Figure 5e). Northern Africa and Eurasia also show weaker $\Delta_n T_s$ increase at critical CO_2 levels (compare 5a and 5c).

The pattern of $\Delta_n P$ from the non-critical CO_2 composite shows the typical "wet gets wetter, dry gets dryer" pattern, whereas at critical CO_2 levels the models show more negative $\Delta_n P$ across the NH (Figures 5b and 5d). Specifically, the NAWH, the tropical Pacific, the subtropical Atlantic, and much of Europe and North Africa show a stronger decrease in P. The model agreement on having negative $\Delta_n P$ over NAWH, Europe, and Northern Africa is also much higher at the critical CO_2 levels (Figure 5b). This highlights the inhomogeneous character of the precipitation response nonlinearity to CO_2 forcing, especially in the Atlantic basin, which is consistent with what is seen in T_s (Figure 5e). In the Pacific, although the P nonlinearity is weak

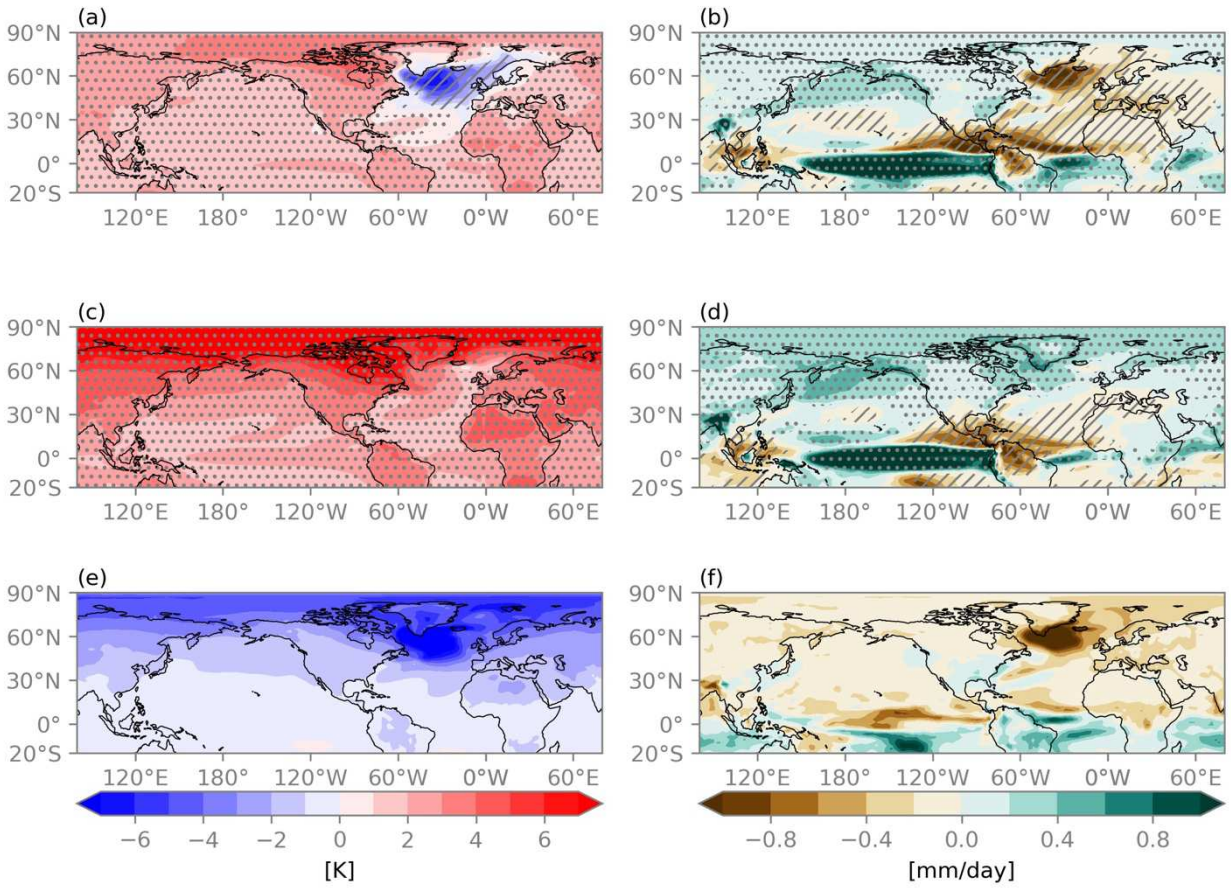

Figure ***5*** Maps of annual-mean surface temperature (left) and precipitation (right) response composites from 8 models with decreased P_{NH} highlighted in Table 1. (a–b) Averaged response at critical CO_2 levels. (c–d) Averaged response at non-critical CO_2 levels. (e–f) Difference between critical and non-critical CO_2 levels. Hatching (stippling) shows agreement of negative (positive) response from 6 out of 8 models.

in the extratropics, we find a dipole reponse in the tropical Pacific that is consistent with a southward ITCZ shift (Figure 5f). These findings suggest far-reaching impacts on *P* outside of the North Atlantic from a collapsed AMOC.

4. Summary and Discussions

We have tested the robustness of the non-monotonic P_{NH} response to increased CO_2 reported for two climate models by Mitevski et al. (2021). Out of 11 couple climate models examined, 8 show a decrease of P_{NH} in response to a doubling of CO_2 concentration. This indicates the non-monotonic response is a common, but not universal, result. Although common, the critical CO_2 level beyond which the P_{NH} decrease occurs differs widely across models, ranging from 2xCO_2 to 8xCO_2 (with an additional simulation in one model showing a decrease for only 1.5xCO_2).

A decrease in T_{NAWH} in response to a doubling of CO_2 is also found in these models, at the same critical CO_2 as for P_{NH}. Furthermore, at this critical CO_2 level we find a collapse of the AMOC, with ψ_{AMOC} weakening by more than 10 Sv for a doubling of CO_2. This suggests that the differences in models' AMOC response can explain their contrasting T_{NAWH} and P_{NH} responses. Models with a large weakening of AMOC for a doubling of CO_2 tend to have cooler NH surface temperature and decreased NH precipitation.

The decrease in NH precipitation at the critical CO_2 occurs primarily over the Atlantic, and extends to Europe and North Africa, but is not confined to the NAWH region. In addition to a P decrease in mid-latitudes, we find a decrease in the subtropics, consistent with a southward shift of the northern edge of the ITCZ. This is consistent with a dynamical strengthening of the NH Hadley cell due to AMOC weakening (R. Zhang & Delworth, 2005; Liu et al., 2017; Orihuela-Pinto et al., 2022; Orbe et al., 2023). While the spatial pattern of simulated precipitation response to climate change is to generally enhance the climatological precipitation pattern (e.g., Held & Soden, 2006), we here highlight the key role of the AMOC response in shaping the global pattern of the precipitation response.

The correlation between the P_{NH} and the ψ_{AMOC} responses to CO_2 doubling suggests that the non-monotonic P_{NH} response to CO_2 increase can be largely attributed to the nonlinear AMOC response. While the NAWH can also form due to atmospheric processes or North Atlantic gyre circulation changes (He et al., 2022; Keil et al., 2020; Li et al., 2022) , its presence is a major fingerprint of the AMOC weakening (Menary & Wood, 2018). Our time series analysis supports this hypothesis, given that the AMOC weakening leads the formation of NAWH and P_{NH} decrease. This is consistent with Bellomo et al. (2021), who found climate models with larger AMOC decline for 4xCO_2 simulations have cooler NH surface temperature and decreased NH precipitation. This conclusion is further supported by multiple North Atlantic "hosing" studies which have analyzed experiments that artificially weaken the AMOC in coupled climate models, and have found precipitation decreases over the NH, particularly in the NAWH region and Europe (Stouffer et al., 2006; Jackson et al., 2015; Liu et al., 2020; Orihuela-Pinto et al., 2022; Bellomo et al., 2023). A weaker AMOC also induces a southward shift of the ITCZ (R. Zhang & Delworth, 2005; Jackson et al., 2015; Moreno-Chamarro et al., 2019), resulting in a dipole response of the tropical Atlantic precipitation (Liu et al., 2017, 2020; Stouffer et al., 2006). Although a detailed discussion of the mechanisms underlying the AMOC-induced precipitation response is beyond the scope of this paper, these earlier studies have noted the roles of thermodynamics, energetics, and storm track dynamics. While we have here focused mainly on NH precipitation, we expect other aspects of the NH response to show similar non-monotonic behavior (Mitevski et al., 2021). For example, nonlinear response in the AMOC has shown to be associated with a nonlinear midlatitude jet response (Bellomo et al., 2021; Orbe et al., 2023; X. Zhang et al., 2023). Subtropical and tropical precipitation is also tightly connected to the Hadley Cell strength and edge location. As demonstrated in M21, both the NH Hadley cell strength and the dry zone edge show non-monotonic behavior similar to P_{NH}. In future work, we plan to explore the monotonicity of other aspects of the climate system response, as well as their connection to the AMOC.

Data availability statement

The post-processed data used in this manuscript can be accessed at the Dryad depository https://doi.org/10.5061/dryad.w0vt4b91x. CMIP6 data can be accessed at https://esgf-node.llnl.gov/search/cmip6/. The Python script used for data processing and plotting are available upon request to the corresponding author.

Acknowledgements

We thank the two anonymous reviewers for their constructive feedback. This work was partially supported by the National Science Foundation awards 2335761 and 1914569. We would like to acknowledge high-performance computing support from the Derecho system (doi:10.5065/qx9a-pg09) provided by the NSF National Center for Atmospheric Research (NCAR), sponsored by the National Science Foundation.

References

Bellomo, K., Angeloni, M., Corti, S., & von Hardenberg, J. (2021). Future climate change shaped by inter-model differences in Atlantic meridional overturning circulation response. *Nature Communications*, *12*(1), Article 1. https://doi.org/10.1038/s41467-021-24015-w

Bellomo, K., Meccia, V. L., D'Agostino, R., Fabiano, F., Larson, S. M., von Hardenberg, J., & Corti, S. (2023). Impacts of a weakened AMOC on precipitation over the Euro-Atlantic region in the EC-Earth3 climate model. *Climate Dynamics*. https://doi.org/10.1007/s00382-023-06754-2

Chadwick, R., & Good, P. (2013). Understanding nonlinear tropical precipitation responses to CO2 forcing. *Geophysical Research Letters*, *40*(18), 4911–4915. https://doi.org/10.1002/grl.50932

Eyring, V., Bony, S., Meehl, G. A., Senior, C. A., Stevens, B., Stouffer, R. J., & Taylor, K. E. (2016). Overview of the Coupled Model Intercomparison Project Phase 6 (CMIP6) experimental design and organization. *Geoscientific Model Development*, *9*(5), 1937–1958. https://doi.org/10.5194/gmd-9-1937-2016

Good, P., Andrews, T., Chadwick, R., Dufresne, J.-L., Gregory, J. M., Lowe, J. A., Schaller, N., & Shiogama, H. (2016). nonlinMIP contribution to CMIP6: Model intercomparison project for non-linear mechanisms: physical basis, experimental design and analysis principles (v1.0). *Geoscientific Model Development*, *9*(11), 4019–4028. https://doi.org/10.5194/gmd-9-4019-2016

Grise, K. M., & Polvani, L. M. (2016). Is climate sensitivity related to dynamical sensitivity? *Journal of Geophysical Research: Atmospheres*, *121*(10), 5159–5176. https://doi.org/10.1002/2015JD024687

He, C., Clement, A. C., Cane, M. A., Murphy, L. N., Klavans, J. M., & Fenske, T. M. (2022). A North Atlantic Warming Hole Without Ocean Circulation. *Geophysical Research Letters*, *49*(19), e2022GL100420. https://doi.org/10.1029/2022GL100420

Held, I. M., & Soden, B. J. (2006). Robust Responses of the Hydrological Cycle to Global Warming. *Journal of Climate*, *19*(21), 5686–5699. https://doi.org/10.1175/JCLI3990.1

Jackson, L. C., Kahana, R., Graham, T., Ringer, M. A., Woollings, T., Mecking, J. V., & Wood, R. A. (2015). Global and European climate impacts of a slowdown of the AMOC in a high resolution GCM. *Climate Dynamics*, *45*(11), 3299–3316. https://doi.org/10.1007/s00382-015-2540-2

Keil, P., Mauritsen, T., Jungclaus, J., Hedemann, C., Olonscheck, D., & Ghosh, R. (2020). Multiple drivers of the North Atlantic warming hole. *Nature Climate Change*, *10*(7), Article 7. https://doi.org/10.1038/s41558-020-0819-8

Li, L., Lozier, M. S., & Li, F. (2022). Century-long cooling trend in subpolar North Atlantic forced by atmosphere: An alternative explanation. *Climate Dynamics*, *58*(9), 2249–2267. https://doi.org/10.1007/s00382-021-06003-4

Liu, W., Fedorov, A. V., Xie, S.-P., & Hu, S. (2020). Climate impacts of a weakened Atlantic Meridional Overturning Circulation in a warming climate. *Science Advances*, *6*(26), eaaz4876. https://doi.org/10.1126/sciadv.aaz4876

Liu, W., Xie, S.-P., Liu, Z., & Zhu, J. (2017). Overlooked possibility of a collapsed Atlantic Meridional Overturning Circulation in warming climate. *Science Advances*, *3*(1), e1601666. https://doi.org/10.1126/sciadv.1601666

Lopez, A., Suckling, E. B., & Smith, L. A. (2014). Robustness of pattern scaled climate change scenarios for adaptation decision support. *Climatic Change*, *122*(4), 555–566. https://doi.org/10.1007/s10584-013-1022-y

Menary, M. B., & Wood, R. A. (2018). An anatomy of the projected North Atlantic warming hole in CMIP5 models. *Climate Dynamics*, *50*(7), 3063–3080. https://doi.org/10.1007/s00382-017-3793-8

Mitevski, I., Dong, Y., Polvani, L. M., Rugenstein, M., & Orbe, C. (2023). Non-Monotonic Feedback Dependence Under Abrupt CO2 Forcing Due To a North Atlantic Pattern Effect. *Geophysical Research Letters*, *50*(14), e2023GL103617. https://doi.org/10.1029/2023GL103617

Mitevski, I., Orbe, C., Chemke, R., Nazarenko, L., & Polvani, L. M. (2021). Non-Monotonic Response of the Climate System to Abrupt CO2 Forcing. *Geophysical Research Letters*, *48*(6), e2020GL090861. https://doi.org/10.1029/2020GL090861

Mitevski, I., Polvani, L. M., & Orbe, C. (2022). Asymmetric Warming/Cooling Response to CO2 Increase/Decrease Mainly Due To Non-Logarithmic Forcing, Not Feedbacks. *Geophysical Research Letters*, *49*(5), e2021GL097133. https://doi.org/10.1029/2021GL097133

Moreno-Chamarro, E., Marshall, J., & Delworth, T. L. (2019). Linking ITCZ Migrations to the AMOC and North Atlantic/Pacific SST Decadal Variability. *Journal of Climate*, *33*(3), 893–905. https://doi.org/10.1175/JCLI-D-19-0258.1

Myhre, G., Highwood, E. J., Shine, K. P., & Stordal, F. (1998). New estimates of radiative forcing due to well mixed greenhouse gases. *Geophysical Research Letters*, *25*(14), 2715–2718. https://doi.org/10.1029/98GL01908

Orbe, C., Rind, D., Miller, R. L., Nazarenko, L., Romanou, A., Jonas, J., Russell, G., Kelley, M., & Schmidt, G. (2023). Atmospheric Response to a Collapse of the North Atlantic Circulation Under A Mid- Range Future Climate Scenario: A Regime Shift in Northern Hemisphere Dynamics. *Journal of Climate*. https://doi.org/10.1175/JCLI-D-22-0841.1

Orbe, C., Rind, D., Waugh, D. W., Jonas, J., Zhang, X., Chiodo, G., Nazarenko, L., & Schmidt, G. A. (2024). *Coupled Stratospheric Ozone and Atlantic Meridional Overturning Circulation Feedbacks on the Northern Hemisphere Midlatitude Jet Response to 4xCO2*. https://doi.org/10.1175/JCLI-D-23-0119.1

Orihuela-Pinto, B., England, M. H., & Taschetto, A. S. (2022). Interbasin and interhemispheric impacts of a collapsed Atlantic Overturning Circulation. *Nature Climate Change*, *12*(6), Article 6. https://doi.org/10.1038/s41558-022-01380-y

Pendergrass, A. G. (2020). The Global-Mean Precipitation Response to CO2-Induced Warming in CMIP6 Models. *Geophysical Research Letters*, *47*(17), e2020GL089964. https://doi.org/10.1029/2020GL089964

Rugenstein, M., Bloch-Johnson, J., Abe-Ouchi, A., Andrews, T., Beyerle, U., Cao, L., Chadha, T., Danabasoglu, G., Dufresne, J.-L., Duan, L., Foujols, M.-A., Frölicher, T., Geoffroy, O., Gregory, J., Knutti, R., Li, C., Marzocchi, A., Mauritsen, T., Menary, M., … Yang, S. (2019). LongRunMIP: Motivation and Design for a

Large Collection of Millennial-Length AOGCM Simulations. *Bulletin of the American Meteorological Society*, *100*(12), 2551–2570. https://doi.org/10.1175/BAMS-D-19-0068.1

Stouffer, R. J., Yin, J., Gregory, J. M., Dixon, K. W., Spelman, M. J., Hurlin, W., Weaver, A. J., Eby, M., Flato, G. M., Hasumi, H., Hu, A., Jungclaus, J. H., Kamenkovich, I. V., Levermann, A., Montoya, M., Murakami, S., Nawrath, S., Oka, A., Peltier, W. R., … Weber, S. L. (2006). Investigating the Causes of the Response of the Thermohaline Circulation to Past and Future Climate Changes. *Journal of Climate*, *19*(8), 1365–1387. https://doi.org/10.1175/JCLI3689.1

Webb, M. J., Andrews, T., Bodas-Salcedo, A., Bony, S., Bretherton, C. S., Chadwick, R., Chepfer, H., Douville, H., Good, P., Kay, J. E., Klein, S. A., Marchand, R., Medeiros, B., Siebesma, A. P., Skinner, C. B., Stevens, B., Tselioudis, G., Tsushima, Y., & Watanabe, M. (2017). The Cloud Feedback Model Intercomparison Project (CFMIP) contribution to CMIP6. *Geoscientific Model Development*, *10*(1), 359–384. https://doi.org/10.5194/gmd-10-359-2017

Zhang, R., & Delworth, T. L. (2005). Simulated Tropical Response to a Substantial Weakening of the Atlantic Thermohaline Circulation. *Journal of Climate*, *18*(12), 1853–1860. https://doi.org/10.1175/JCLI3460.1

Zhang, X., Waugh, D. W., & Orbe, C. (2023). Dependence of Northern Hemisphere Tropospheric Transport on the Midlatitude Jet Under Abrupt CO2 Increase. *Journal of Geophysical Research: Atmospheres*, *128*(13), e2022JD038454. https://doi.org/10.1029/2022JD038454